Water Practice & Technology

IWA PUBLISHING

Water Practice & Technology Vol 19 No 3, 960 doi: 10.2166/wpt.2024.044

Effect of hydrological variability on suspended sediment load at a river junction: a case study

Nabina Khanam and Sushant Kumar Biswal*

Department of Civil Engineering, National Institute of Technology Agartala, Tripura, India
*Corresponding author. E-mail: drsushant.civil@nita.ac.in

ABSTRACT

Confluences act as crucial intersection in a fluvial system as they regulate the flow, sediment, and geomorphological stability. Two of the natural occurrences that have an effect on hydro-morphological processes that characterize the channel are sediment movement and stream discharge. However, assessments of suspended sediment distribution patterns across channel confluences and functions of tributaries on sediment transfer in downstream streams are still inadequately explored. To fulfil this, a year-long field investigation was conducted around river confluence at various time scales during the hydrological season. The bathymetry of the confluence was performed using digital echo-sounding equipment, electro-magnetic current meter, and differential global positioning equipment. This study uses in situ measurement and empirical techniques to quantify the spatiotemporal distribution of suspended sediment particles. Furthermore, Yang's formula was used to analyze the sediment concentration, and several statistical standards were employed to establish a differentiation between predicted and observed data. The results illustrated that a good agreement has been achieved among the calculated and measured statistics based on the correlation coefficient value. According to the findings, 8% fewer errors in the quantification of suspended sediment were induced in the tributary than in the main river because of the very low flow of the tributary. The present ramifications can help increase our database and understanding of the dynamics of major river confluences.

Key words: confluence, field study, suspended load, suspended sediment concentration, Yang's formula

HIGHLIGHTS

- A year-long field investigation was carried out to assess short-term suspended sediment rates and stream flow rates.
- Statistical analysis was concluded between observed and predicted data.
- The grain size of bed material varied significantly among individual channels in a variety of fluvial circumstances.
- The tributary channel reflects the fluctuations along the longitudinal gradient of sediment rate.

1. INTRODUCTION

River junctions are realized as important fluvial characteristics since both thorough and widespread hydro-physical and geo-ecological processes occur at this junction (Rice *et al.* 2008; Edward & Latrubesse 2015; Yuan *et al.* 2019; Gualtieri *et al.* 2020). Hydro-morphodynamics in rivers of any size (large- or small-scale rivers) are unpredictable and complex, mainly in river networks where flows converge or diverge (Parsons *et al.* 2007; Leite Ribeiro *et al.* 2012; Constantinescu *et al.* 2016). Significant modifications in flow hydrodynamics, bed morphology, and environmental and ecological features happen at confluence due to the possible mixing of the sediment and pollutants from separate flows, adjusting to the post-confluence planform geometry (Nazari-Giglou *et al.* 2016; Tang *et al.* 2018; Gualtieri *et al.* 2019; Rhoads 2020; Yuan *et al.* 2022). Numerous academic fields, inclusive of sedimentology (e.g. Constantinescu *et al.* 2012; Zhang *et al.* 2014; Rhoads & Johnson 2018), hydraulics (Constantinescu *et al.* 2012, 2016; Sukhodolov & Sukhodolova 2019); and ecology (Benda *et al.* 2004; Blettler *et al.* 2014) have attempted to comprehend the function of fluvial networks. Confluences are naturally occurring elements in river network systems that control the movement of flow, sediment, and geomorphological stability. It is crucial to predict the large amount of sediment loads slightly more precisely corresponding to the carrying capacity of the river, especially for river networks. Various planform geometries, velocity ratios, bed discordance, and junction angles were used to assess the movement of sediments in river systems (Riley *et al.* 2014; Guillen Ludena *et al.* 2017; Sukhodolov *et al.* 2017; Lyubimova *et al.* 2020; Rhoads 2020). The fluctuation of the

mixed flows at the surface level in the junction relies upon the streamflow condition and the annual hydrological regime. The structure and extent of river flow are changed owing to varying rainfall patterns, and this has an impact on sediment yield and transport patterns of sediment from tropical river basins. The dispersal of suspended sediment in the channel junction is influenced by the sediment deliveries over the main and lateral flows. The flow discharge and sediment discharge undergo drastic variations at the junctions (Szupiany *et al.* 2012; Khosronejad *et al.* 2016), which necessitate adjusting the interdependent channel form factors. The abrupt adaptation in the hydro-sedimentological environment of the receiver stream brought on by the tributary inflow of water and sediment at river junctions results in changes in physical conditions (Biron & Lane 2008). Although the tributaries have usual basin characteristics and their linking with the major stream changes in the sedimentation that causes the hydro-morphological alteration of the receiving downstream river. Therefore, the inputs and contributions of the tributaries have a significant impact on the concentrations of suspended sediment characteristics within the downstream channel. Quantifying the sediment load in the streams is one of the major fluvial issues that scientists are currently dealing with because it directly influences several hydro- morphological problems in channel beds. According to numerous empirical equations that are available or from actual quantification of sediment taken around the timespan, the suspended sediment load (SSL) of the stream is typically approximated by Khanchoul *et al.* (2009). However, it continues to be a major issue for researchers to estimate SSL in small rivers with fast discharge changes.

Numerous studies have been undertaken in the past by Ferguson & Hoey (2008), Espinoza *et al.* (2012), Guillen Ludena *et al.* (2017), Gualtieri *et al.* (2018) to recognize the procedures intricate in motion of sediment through the estuary and the river network system. To examine the relationship among flow dynamics and bed morphology with downstream stream (Ragno *et al.* 2021), field investigations (Rhoads *et al.* 2009; Riley *et al.* 2014; Sukhodolov *et al.* 2017; Ianniruberto *et al.* 2018; Lane *et al*. 2008; Lewis *et al.* 2020; Yuan *et al.* 2021, 2022), laboratory tests (Escauriaza *et al.* 2012; Guillen Ludena *et al.* 2017; Cheng & Constantinescu 2018; Yuan *et al.* 2018; Wang *et al.* 2019; Yu *et al.* 2020; Zhang & Lin 2021; Balouchi *et al.* 2022) and modelling (Baranya & Jozsa 2013; Sukhodolov *et al.* 2017; Jiang *et al.* 2022) were carried out. At the junction of the Parana and Paraguay Rivers, measurements from a field survey by Parsons *et al.* (2007) showed how the cross-sectional velocity dispersion affects the flow and suspended bed sediment concentration, with the effect becoming more pronounced as the aspect ratio (W/H) of the channels rises. Confluences are highlighted as a site of discontinuance in the hydro-sediment continuance in a river system (Rice *et al.* 2008; Duncan *et al.* 2009). The studies of hydro-sediment dynamics and associated problems in the junction hydrodynamic region through Leite Ribeiro *et al.* (2012), Martín-Vide *et al.* (2015), and Nazari-Giglou *et al.* (2016) are significant in this context. According to Szupiany *et al.* (2012), the characteristics of rivers, like the development of islands, the growth of sizable lateral bars, and the presence of turbulent zones, might affect the transport of sediment. Artificial neural networks (ANNs) and machine learning (ML) were used by Tachi *et al.* (2016) to estimate suspended sediment discharge, but these methods did not demonstrate accuracy in forecasting suspended sediment concentration (SSC) based on the flow rate. The intricate interplay between water output and sediment concentration made it impossible to forecast SSC using artificial methods.

Literature surveys have developed our perception of the trend of riverine suspended sediment loads; however, our understanding of suspended sediment motion in these rivers is very limited. Accurately measuring sediment loads in alluvial rivers is a challenging and unrealistic task, which significantly impedes our knowledge. In most alluvial rivers, it is difficult and rare to acquire direct measurements of sediment transport, because sand and other particles of various sizes are typically combined with sediments. Following the review of the literature, it was found that no thorough research has been completed on the dynamics of suspended sediment transfer, or the movement of sediment in the water column, from any perspective, particularly with regard to the impact of unsteady rainfall and river discharge on sediment concentrations. So far, the quantification of the post-confluence channel's suspended sediment distribution patterns is still not realized. Therefore, it is necessary to assess the suspended sediment discharge under various hydraulic conditions at the junctions. This study examines the spatiotemporal changeability of suspended sediment distribution and estimates SSL for certain time periods following a junction over several hydrological seasons by employing both field measurement and empirical methods. In the present study, field data from the Gumti River and Pitragang tributary are used to calculate the total suspended sediment (TSS) transport rate using method of Yang (1979). Thus, it is hoped that a thorough investigation of this confluence would contribute to our understanding of river confluences and facilitate the better direction of this crucial river network system.

2. MATERIALS AND METHODS

2.1. Study area

Gumti River is the longest river (164 km) in Tripura, India. It is located at the junction of the Gumti River and the Pitraganja tributary with a basin area of 174 km^2 and considered for seven percent of the Gumti River basin area (2, 492 km^2). The study area extends from latitude 23°32′N to 23°47′N and longitude 91°14′E to 91°58′E. The stream's annual mean rainfall is 2,625 mm and its average temperature is 30.5 °C. At the study site, there is an annual water discharge of 10.50 m^3/s, with a sediment concentration of 65 mg/l, a normal flow depth of 1.45 m, a maximum flow depth of 1.78 m, and a high flood level of 2.42 m. The location of the study area is depicted in Figure 1. The length and accessibility of river discharge, river stage and sedimentation

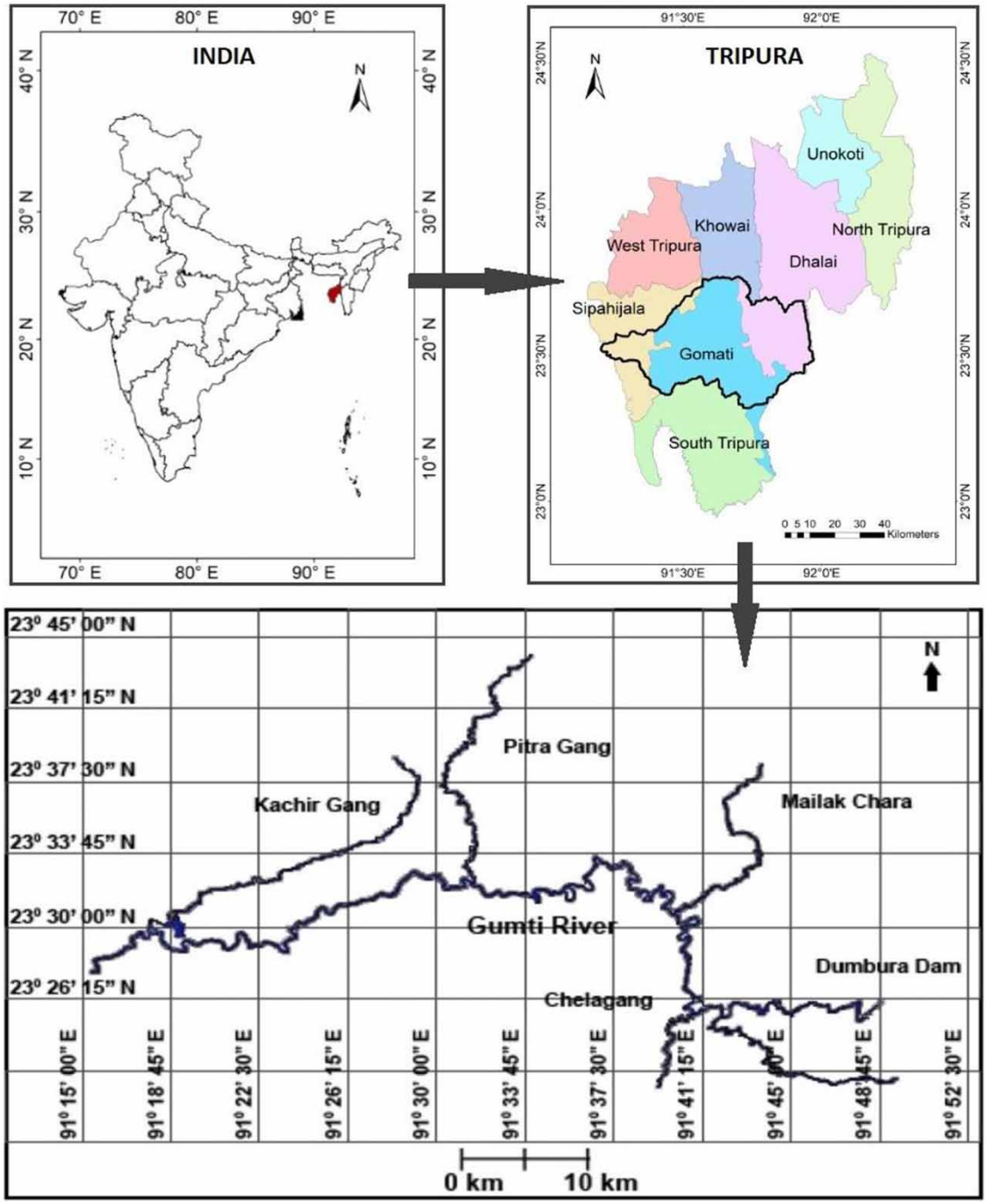

Figure 1 | Schematic map of the study area.

appropriate for this survey fluctuate with environmental seasons, and this site was solely used for the estimation of suspended loads.

2.2. Field procedures

The bathymetric survey of the confluence was carried out to assess short-term suspended sediment rates and stream flow rates in a variety of hydrologic circumstances. In this study, selected sampling locations in the Gumti-Pitragang junction were used to collect and analyze data including river discharge, suspended sediment, sediment particle-size distribution, and water chemistry parameters. To undertake this, between February 2021 and February 2022, five field campaigns were used for 30 days of survey measurements spaced 2 months apart under diverse climatic circumstances. The survey was prolonged from the apex of the junction to a length of 500 m upstream in both channels and 2,000 m downstream. This reach was divided into a total of 14 cross-sections for the two branch channels (every 2 cross-sections) and the post-confluence (10 cross-sections) which were spaced 200 m apart (Figure 2). The cross-sections were divided into three equal portions. The width of the confluence at its apex is 110 m wide and 85 m further downstream. The main river is approached by the tributary channel at an angle of 82 degrees. The bathymetry of the confluence was performed through the use of an electro-magnetic current meter, digital echo-sounding equipment and differential global positioning service equipment. All measurements were georeferenced employing a differential global positioning system (DGPS). Between June and September, the river experienced floods, but the flow remained low for the rest of the year. The flow of the rivers is more dominant during the flood period than in other periods. So, all the measurements are made after the flood has receded. The schematic diagram (Figure 2) illustrates the places in transects of the two branch channels and in the post-confluence for hydraulic data gathering. The cross-sectional area-velocity approach was used to measure river discharges. Following measurements of the river's sectional widths and depths, cross-sectional areas were calculated. During the whole-field survey, 108 discharge measurements were completed. At a particular location, the slope of the river bed between two consecutive cross-sections is determined by the difference between their elevations (higher-lower) divided by the distance between them. In this study, the average river bed slopes were determined for every location during 2021–2022. The geometrical and mean hydraulic properties of the confluence are demonstrated in Table 1.

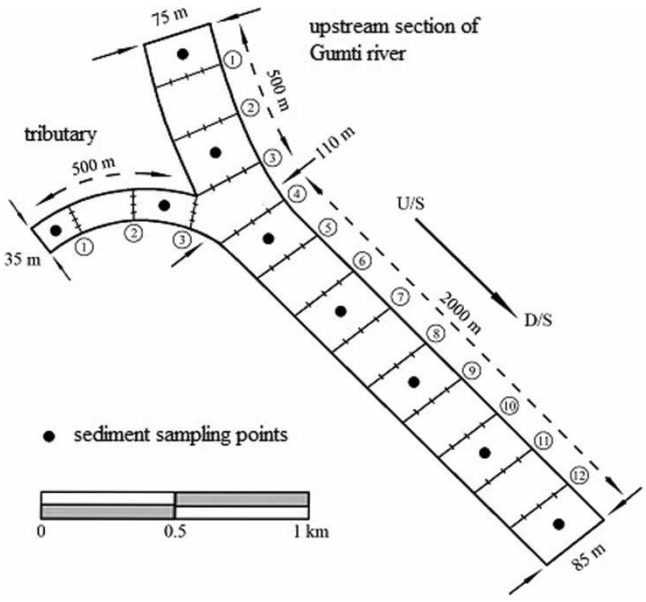

Figure 2 | Schematic sketches of measurement cross-sections showing the sampling locations.

The flow velocity for each of the sections (V_i) was assessed employing an electro-magnetic current meter, and water levels were recorded using a depth echosounder and staff gauge. The river discharges (Q_i) for each of the sections were evaluated by multiplying sectional depths (h_i) and widths (W_i) to obtain cross-sectional areas (A_i)

Table 1 | Dimension and average hydraulic parameters of the junction at the time of bathymetric survey

Channel	W (m)	H (m)	$Q(m^3/s)$	$\bar{U}(m/s)$	$S \times 10^{-3}$	W/H	Momentum flux, $M = \rho Q\bar{U}(kgm/s^2)$	$Fr = \bar{U}/\sqrt{gD_h}$	$Re = \rho\bar{U}D_h/\mu \times 10^6$
Main (U/S)	75.46	1.518	87.93	0.768	0.58	49.71	67,497	0.198	2.31
Main (D/S)	84.92	1.451	109.06	0.885	0.63	58.53	96,528	0.235	2.55
Tributary	35.18	0.914	20.98	0.652	0.61	38.49	13,689	0.218	1.18

which were later multiplied with the average velocity of flow ($\bar{V}_i$) at the section as shown in Equation (1).

$$Q_i = \sum_{i=1}^{n} W_i h_i \left(\frac{V_i + V_n}{n}\right) \tag{1}$$

$$Q_i = \sum_{i=1}^{n} A_i \bar{V}_i \tag{2}$$

The total river discharge (Q_d) was acquired by summing up the flow rates obtained at the sub-sections (Q_i) for the river transects as shown in Equation (3).

$$Q_d = \sum_{i=1}^{n} Q_i \tag{3}$$

Here, W is the width of rivers (m), H is the water height (m), Q is the discharge in (m^3s^{-1}), $\bar{U}$ is the mean flow velocity (ms^{-1}), ρ is the water density (Kgm^{-3}), μ is the viscosity of water ($Kgm^{-1}s^{-1}$), S is the slope of confluence channel, D_h is the hydraulic depth (m), M is the momentum flux ($Kgms^{-2}$), Fr is Froude number of flow, Re is Reynolds number of flow, and W/H is the aspect ratio.

To capture fluctuations in sediment influx, the collection dates were dispersed throughout those months. GPS coordinates were obtained for each sampling station at the chosen confluence location, in order to collect the water quality data in the same place at various times. Water samples are taken at three distinct depths (such as the surface, 40 and 80 cm) at several sampling points at the confluence in the middle of each section. A total 540 number of samples are gathered throughout the field campaign. It is believed that the sampling records are reliable and impartial throughout the sampling period at suitable locations, regardless of the seasons and flow regimes. These water samples were utilized to determine the local TSS concentration values and to gain insight into the temperature, pH, and conductivity of the post-confluence (Table 2). Depending on the river flows and the properties of the sediment, water samples were collected every 2 h from each station by a Nansen bottle, and the temperature of the water was recorded using a Multimeter MM 40 device (Crison Instrument). The parameters were evaluated using a water quality meter, and the turbidity of the river water sample was assessed using a Nephelo turbidity meter in the environmental laboratory. In the current work, water SSC samples are collected from a limited number of selected stations that do not represent the entire river locations, with the exception of rainy days in the field. The confluence of the Gumti and Pitragang River demonstrates the variations in their physio-chemical and hydraulic properties. The laboratory test results indicate that the pH of the water sample collected from a river was found to be acidic. However, the nominal SSC values were recorded in February 2022;

Table 2 | Mean water quality parameters at the confluence downstream

Sl. no.	Temperature (°C)	Conductivity (μS/cm)	Turbidity (NTU)	pH	SSC (mg/l)
15–20 Feb 2021	28.4	134	102	7.2	121
24–30 May 2021	29.3	207	136	7.8	185
18–23 Aug 2021	28.1	232	158	8.2	194
14–19 Nov 2021	27.8	189	113	8.0	170
17–22 Feb 2022	28.1	116	97	7.5	104

this could be due to the Gumti River experiencing more dilution owing to the contribution of tributaries free of suspended sediments. In the interval between May and August, the SSC rises from 185 to 194 mg/l (Figure 3).

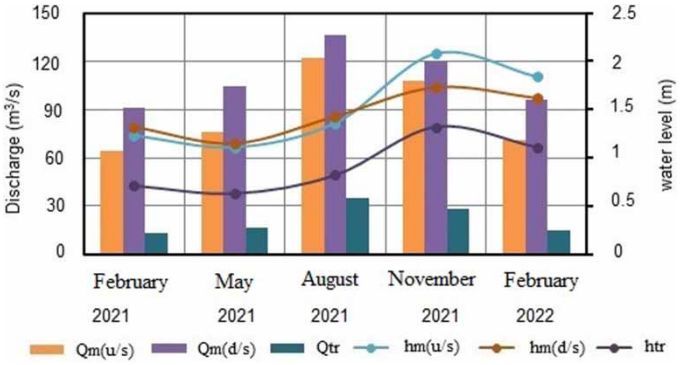

Figure 3 | Water levels were observed during the field study period (February 2021 and February 2022).

2.3. Grain size particle

This work was intended to determine the grain size distribution (GSD) of the bed materials, thus samples were regularly taken from the river bed next to the channels. The samples are collected from tributaries to the downstream of the confluence covering approximately a 2,500 m stretch of water streams. In order to examine the spatial shape of grain features regularly between sampling days, subsurface materials of 50–80 kg samples were collected one time from the identical location. Using a stainless steel grab sampler, sediment samples were collected at each sampling location and then promptly closed in an air-tight container. Prior to physical sieving, the samples were kept in laboratory tray and dried in an oven at 105 °C for 24 h. Sieving was done in the laboratory by an electric sieve shaker to analyze the variations of the GSD smaller than 0.075 mm and up to 4.75 mm for each of the sampling places. Figure 4 displays the GSD for each sample on the log-log scale. Sieve analysis becomes accompanied by hydrometer evaluation on 50-gram soil samples finer than 0.075 mm to carry out the category of finer particles. This fraction becomes shaken for 30 min with 20 ml of sodium hexa-metaphosphate solution and 200 ml of distilled water. For the hydrometric study, 800 ml of pure water was added and the mixture was kept in a constant temperature bath for 48 h. Table 3 illustrates the percentage of clay, silt and sand fractions of field-based experiments for each branch channel. To comprehend the hydrodynamic characteristics of relevant sediment locations and relate the sedimentation process, GSD offers crucial information on sediment mobility and accumulation (Zhang *et al.* 2015). According to the grain size of the particle, sand is categorized as fine sand (0.075–0.425 mm), medium sand (0.425–2 mm), and coarse sand (2.0–4.75 mm). The bed materials used in this study, which were collected from various selected areas, had smaller grain sizes ranging from 0.17 to 0.41 mm, falling into the category of fine sand based on the grain size of the particle. For the purposes of this study, the sediment density is assumed to be a default value of 2,650 kg/m^3 to for the entire study because the river bed at the junction is composed entirely of sandy material.

2.4. Measurement of SSL

2.4.1. Direct method

Characterizing the suspended sediment concentrations (SSC) and suspended sediment loads (SSL) under a variety of stream flow conditions at specific locations within the research area is one of the objectives of collecting the suspended sediment data. Sampling was undertaken throughout the bathymetric period in order to analyze the SSC and GSD. Upstream of the tributary and downstream of the confluence were used as sample sections of the channel confluence to collect sediment samples. In this investigation, a total of 540 water samples for SSC were taken at three different depths (e.g. at the surface, 40 and 80 cm) on each section from the center of the cross-section at different sampling stations about confluence. Three to six samples were taken in one vertical profile, depending on the depth of the water. The pre-monsoon periods (February – May), monsoon (June-September), and post-monsoon (October – January) periods are used to measure the sediment influxes under steady flow conditions at the confluences. At each sampling location, a litre of surface water was collected in a Nansen bottle. A Whatman 320 mm diameter filter paper with a 0.45 μm (particle retention) filter was used

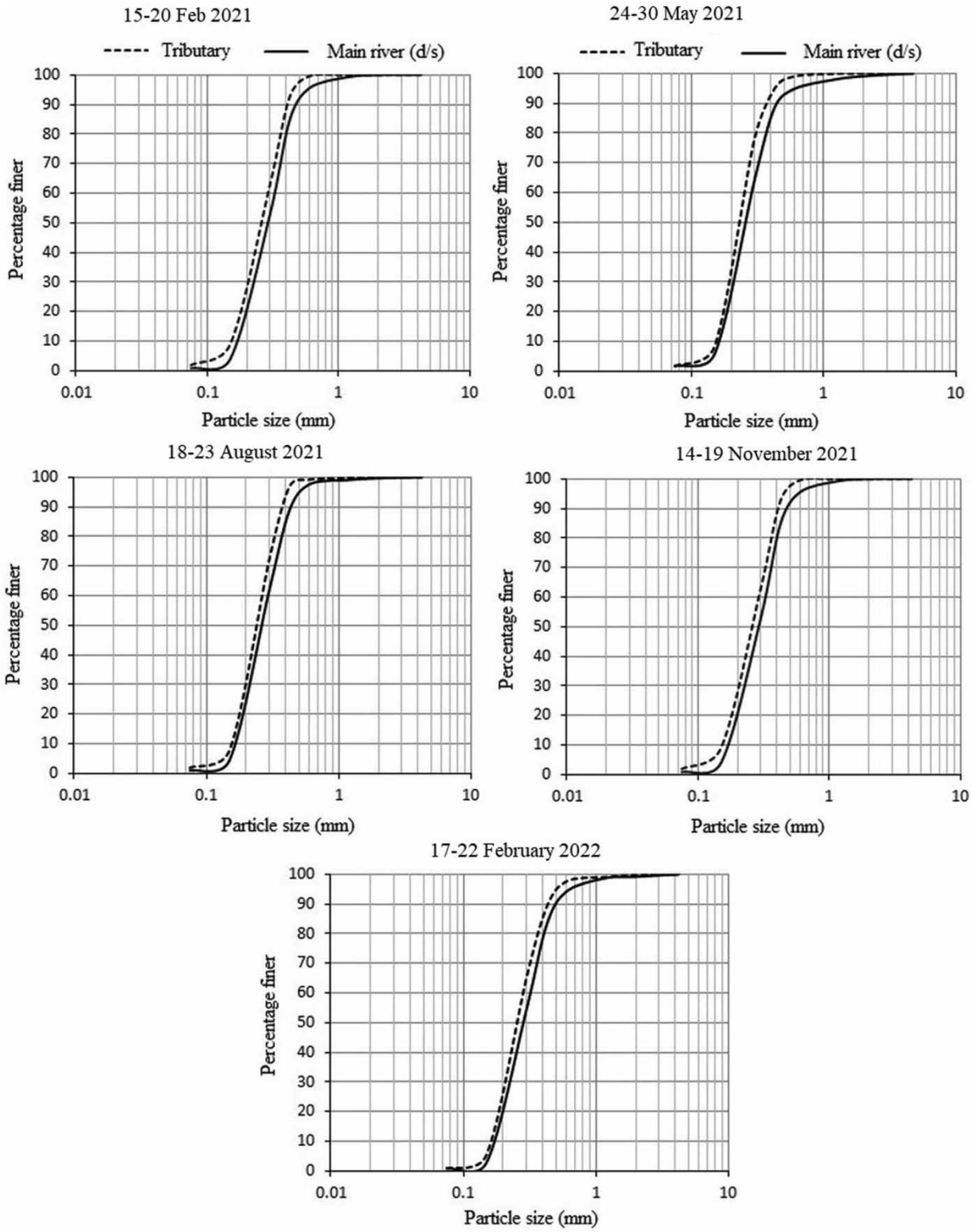

Figure 4 | Grain size distribution (GSD) curves of samples.

to filter the sampling for determining the SSC. The retained mass of the sample was then parched in an oven for 24 h at 105 °C to calculate the net weight of the suspended load. As a result, the SSC was computed from the difference in the initial and final weights of filters divided by the weight of water in the sample. The sampling and filtering techniques follow those outlined by the World Meteorological Organization (WMO) and the

Table 3 | Percentages of clay, silt, and sand fractions for each branch channel

	% soil		
Branch channels	**Clay** < **0.002**	**Silt (mm) 0.002–0.0475**	**Sand 0.0475–2**
Tributary	1.04	4.68	94.28
Main channel (U/S)	1.52	5.44	93.04
Main channel (D/S)	1.76	7.31	90.93

Global Environmental Monitoring System (GEMS). Calculations of suspended sediment discharge, or load, in g/s or (tons)/day were made possible by collecting stream discharge data concurrently with SSC data. The formula used to determine the discharges of suspended sediment was as follows (Gray & Simoes 2008; Gray *et al.* 2015):

$$Q_S = Q.C_S \tag{4}$$

where Q_S is the suspended sediment discharge expressed in g/s; Q is the stream discharge (m^3/s); and C_S is the suspended sediment concentration (mg/l).

2.4.2. Empirical method

In this study, sediment concentrations were determined by applying formulae of Yang (1979) using 540 datasets of measured stream discharge around the confluence of the Gumti River. This made it possible to compare total sediment concentrations that were computed and site-measured. Yang's formula was used to determine the total suspended transport rate as a function of hydraulic variables such as flow velocity, critical flow velocity, grain diameter, and settling velocity. Yang's expression is a hydraulic method for solving the issue of sediment transport. In this work, a single fraction of grain size is used to calculate the sediment transport rate of the basic material based on Yang's Formula. The various nonlinear regression equations in Yang's formulations were linearized for this investigation. The following is the Yang's expression for the TSS movement in a river:

$$Q_s = \gamma_w H\bar{U}(C \times 10^{-6}) \tag{5}$$

From the Equation (6), the total sediment concentration is calculated as follows:

$$\begin{aligned}\log C = {} & 5.165 - 0.153\log\frac{w_s d_{50}}{\nu} - 0.297\log\frac{u_*}{w_s} \\ & + \left(1.780 - 0.360\log\frac{w_s d_{50}}{\nu} - 0.480\log\frac{u_*}{w_s}\right)\log\left(\frac{uS}{w_s}\right)\end{aligned} \tag{6}$$

where C is the total sediment concentration in (mg/l) by weight; γ_w is the unit weight of water (kN/m^3); w_s is the terminal fall velocity of sediment particles (m/s); d_{50} is the median particle diameter (m); S is the channel slope; and u_* is the shear velocity (m/s). Yang's formula can be expressed as an equation for multiple linear regressions that take into account the auxiliary variables x_1, x_2, x_3, x_4 andx_5 that are considered.

$$\begin{aligned} x_1 &= log(w_s d_{50}/\nu) \\ x_2 &= log(u_*/w_s) \\ x_3 &= log(uS/w_s) \\ x_4 &= log(uS/w_s)log(w_s d_{50}/\nu) \\ x_5 &= log(uS/w_s)log(u_*/w_s) \end{aligned} \tag{7}$$

Equation (6) can be written as a linear multiple regression equation:

$$logC = 5.165 - 0.153x_1 - 0.297x_2 + 1.780x_3 - 0.360x_4 - 0.480x_5 \quad (8)$$

3. RESULTS AND DISCUSSION

3.1. Comparison between predicted and observed sediment concentration

At first glance, it seems that a minor difference in expected suspended sediment concentration between the two different methodologies (i.e. field data and computer data). Therefore, a statistical analysis is required to identify the specific distinctions between them. The accuracy of the predicted method was statistically analyzed by comparing it with observed data. Calculations for the mean absolute percentage error (MAPE), root mean square error (RMSE), Nash–Sutcliffe efficiency (NSE), and linear correlation coefficient were made as part of the statistical study (Table 4). The following equations are used to generate these statistical measures (Krause *et al.* 2005; Najafzadeh & Tafarojnoruz 2016). At this point, it is emphasized that Yang's calculations were used to get the overall sediment concentration.

Table 4 | Measured and derived statistical criteria for the confluence river

Channel	Months/Statistical criteria	15–20 Feb 2021	24–30 May 2021	18–23 Aug 2021	14–19 Nov 2021	17–22 Feb 2022	Mean value
MC	MAPE	0.285	0.744	0.898	0.995	0.337	0.652
TC		0.431	0.672	0.414	0.372	0.524	0.483
MC	RMSE	10.58	23.31	37.12	29.61	10.43	23.21
TC		8.14	12.53	12.88	17.35	8.02	11.78
MC	NSE	0.481	–2.092	−4.596	−2.884	−0.342	−1.887
TC		−1.148	−2.975	−0.309	−1.453	−2.697	−1.716
MC	r	0.923	0.883	0.879	0.952	0.771	0.882
TC		0.937	0.944	0.896	0.857	0.858	0.898
MC	R^2	0.851	0.739	0.773	0.929	0.894	0.837
TC		0.878	0.891	0.826	0.803	0.806	0.841

MC, main channel; TC, tributary channel.

Mean Absolute Percentage Error (MAPE, (%))

$$\text{MAPE} = \frac{1}{N}\sum_{i=1}^{N}\left|\frac{x_{io} - x_{ip}}{x_{io}}\right| \quad (9)$$

The MAPE is an indicator of the quality of the approximation between predicted and measured values, given the magnitude of the actual quantity value. It is considered that the prediction is reasonably accurate if the MAPE value is less than 5%. When the MAPE is more than 10% but less than 25%, the accuracy is poor but acceptable, and when the MAPE is more than 25%, the accuracy is extremely low.

Root Mean Square Error (RMSE)

$$\text{RMSE} = \sqrt{\sum_{i=1}^{N}(x_{i0} - x_{ip})^2/N} \quad (10)$$

The RMSE computes the average discrepancy between the values predicted by a model and the actual values. It provides an estimate of the model's accuracy or how effectively it can anticipate the desired outcome. The RMSE ranges between 0 and $+\infty$. The correlation between measured and calculated values improves with a lower RMSE.

Nash –Sutcliffe Efficiency (NSE)

$$\mathrm{NSE} = 1 - \frac{\sum_{i=1}^{N} (x_{i0} - x_{ip})^2}{\sum_{i=1}^{N} (x_{io} - \overline{x_o})^2} \tag{11}$$

NSE can be quantitatively defined by the correctness of model outputs. NSE ranges from $-\infty$ to 1, with 1 being the optimal value.

Linear Correlation Coefficient (r)

$$r = \frac{\sum_{i=1}^{N} (x_{io} - \bar{x}_o)(x_{iP} - \bar{x}_p)}{\sqrt{\sum_{i=1}^{N} (x_{i0} - \bar{x}_0)^2} \sqrt{\sum_{i=1}^{N} (x_{ip} - \bar{x}_p)^2}} \tag{12}$$

Correlation coefficient r expresses the degree of mutual linear dependence between the variables x_{io} and x_{ip}, and ranges between values of -1 and $+1$. Here x_{i0} is the measured sediment concentration; x_{ip} is the predicted sediment concentration; $\bar{x}_0$ is the average value of x_{i0} ; $\bar{x}_p$ is the mean value of x_{ip} and N is the number of data.

The magnitudes of the RMSE and NSE, supported the Yang's formula, can be considered to be rather satisfactory in the comparison between the observed and predicted approaches for the channel confluence described above. Also acceptable is the degree of linear dependency amid the predicted and the observed sediment concentration. The outcomes indicate that the values of NSE are clearly non-negative and there is a better identical between observed and predicted SSC with a mean determination coefficient of $R^2 = 0.84$. The MAPE value for both predicted and measured values is less than 1% suggesting a high level of performance and accuracy in the anticipated results. According to the statistical requirements of this study, which are displayed in Table 4, Yang's approach adequately describes the suspended sediment concentrations in the Gumti and Pitragang rivers, and the findings are adequate.

Another important finding from this study is that, with average water discharge of 21 $m^3 s^{-1}$ the amount of suspended sediment that reaches the entrance of the confluence is rather small roughly 85 ton/year. During the bathymetric survey, the downstream tributary and Gumti River had mean SSC of 46 and 94 mg/l, respectively. The highest amount of suspended sediment was observed in August in the main river and in November in the tributary (Table 5). The performance of the results is based on a comparison of the quantification of suspended sediment yields applying two separate methods. The results emerging from empirical formulas usually differ from the measured data. In the current work, the empirical formula uses a mathematical formula to estimate the sediment load of the dataset based on sample data. The direct approach uses a dataset to calculate the SSL without making any assumptions. Although, the direct method is expensive, time-consuming and laborious. However, compared to the empirical method, the direct method is significantly more exact and accurate. The primary cause of error for the direct method was due to the heterogeneity of samples collected from the river, and a large enough spatial and temporal variation of the concentration and rate of sediment transport. This error source was random and could not be eliminated. In the present study, the relative error of the empirical method was 6.23%, while, the relative error of the direct method was less than 3.15%. Moreover, the difference in suspended sediment rate is dependent on the extent to which its tributary has an impact. There were eight percentages (8%) fewer errors in the quantification of suspended sediment induced in the tributary than in the main river because of the very low flow of the tributary. Fewer errors were found in the analysis of suspended sediment generated during the cloudy period than in the dry period.

Table 5 | Shows the observed and predicted suspended sediment transport rate (g/s)

Channel/Months	Results	15–20 Feb 2021	24–30 May 2021	18–23 Aug 2021	14–19 Nov 2021	17–22 Feb 2022	Mean (g/s)
Main	Calculated	379	764	1,070	736	260	642
	Observed	304	458	885	371	192	442
Tributary	Calculated	42	54	116	140	61	83
	Observed	28	30	84	103	43	58

3.2. Suspended sediment transport and sediment discharge

Secondary currents, turbulent diffusion, and entrainment from the channel bed all had a crucial role in calculating the sediment concentration. Sediment concentration typically rises downstream as a result of the continued inclusion of ruined material from various tributaries and non-point sources. Furthermore, surface water mixing along the main channel relies on the hydrological period that has the maximum mixed homogenized area observed during peak water discharge season and the lowest during the rising discharge season. The discrepancy between flow and sediment concentration indicates certain basic distinctions between the momentum and sediment transfer systems. This may be owing to the occurrence of secondary flows and, to a lesser extent, large-scale coherent structures (e.g. shear-induced KH instability at the mixing interface). Figure 5 show the scatter plot of measured and predicted suspended sediment concentration rate.

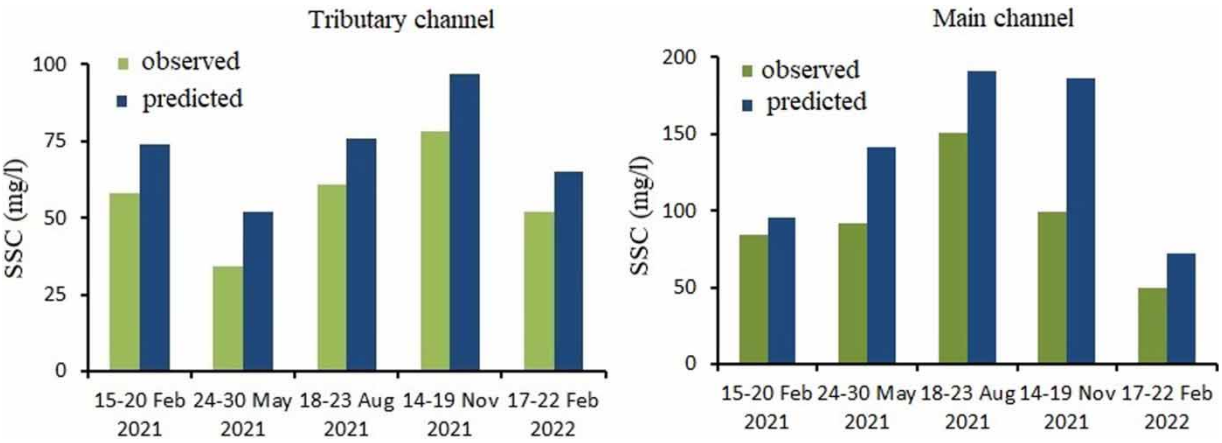

Figure 5 | Shows the average value of SSC as computed and observed.

Based on the present study, two factors of interest that are believed to have fundamental effects on the confluence hydrodynamic zone (CHZ) are hypothesized to be tributary sediment yield and runoff volume. The study affirms that the dimension of the tributary compared to the mainstream affects sediment movement inside the CHZ of the main channel. Furthermore, the suspended load estimation suggests that notable spatiotemporal changeability can happen in sediment supplies from upstream to downstream reach of confluence. The yearly hydrological regime had an impact on the water mixture in August 2021; water mixing rates were highest followed by those in June and October. It is probable that the tributary was carrying clay (of which 1% were smaller than 0.002 mm), suspended silt (of which 5% were less than 0.05 mm) and sand (94%). On the other hand, the Gumti River was carrying some clay (of which 2% were smaller than 0.002 mm), silt (of which 7% of the particles were less than 0.05 mm), and fine sand (91%) (Figure 4). The average grain size of the suspended particles was identical in the Gumti River and Pitragang tributary. However, the grain size of bed material varied significantly among individual channels. The mean grain size of the tributary was only 0.27 mm and its bed material was much finer than that of the main river. The tributary river experienced severe erosion due to the increased suspended load during the high velocity survey periods.

According to the field findings, the velocity is always higher instantly downstream of the confluence than immediately upstream. Owing to the reduction of the water level, the flow in the left branch attained a high velocity and maintained a higher TSS content than what was seen during high-flow circumstances. The converging flows of the two confluent channels magnified cross-sectional velocity and carried a substantially higher sediment load (e.g. 442 mg/l), which was likely caused by bed sediment resuspension. The TSS concentration at the mixing interface was measured at around 152 mg/l. The suspended load is merged and mixed with the masses of the two branches of the confluence river. At CHZ, sediment from the left branch of the Gumti River, which had a low sediment concentration combined with the right branch. The mixing of Gumti and Pitragang sediment was hindered with minimal mixing before the CHZ and no complete mixing visible downstream of the CHZ. The sediment could not be dispersed uniformly across the section due to downwelling flow. Further downstream at CHZ, the suspended sediment had not completely mixed. The concentration of the sediments in these flows decreased to 56 mg/l at CHZ after being mixed, which is a significant decrease from the concentration upon

arrival from the Pitragang tributary. It is essential to note that, in most of the sample campaigns in the post-confluence channel, the discharge increase ranges between 5 and 38%. The rise in sediment content, cross-sectional area, and hydraulic radius that occurred after the confluence point, ranging from 9.72% to 28.78%, maybe the cause of this deviation. At the outlet, it was observed that there is more suspended sediment movement on the left banks of the Gumti River. The total sediment flux of Gumti River indicates retention of 18% suspended load due to the shallow water gradient and lowered flow velocity caused owing to the backwater effect of Gumti River on the Tributary River (Figure 6). The hydro-sedimentation scenario of the Gumti River's low course described in this work suggests a gradual and ongoing process of sedimentation in the confluence area. According to the findings, the tributary has an impact on the main river's discharge of suspended sediment by increasing it by 8%. It is clear that the SSL for specific areas following the junction is notably larger than that of the upstream.

3.3. Uncertainty and constraints in suspended load estimation

The calculation of sediment loads (Q = suspended load, Qs + bed load, Qb) in this work is to quantify SSL Qs repeatedly along transects in river confluences over a 1-year period. Most previous studies that quantified sediment loads along the large river made use of 2D or 3D models that included bedform contour height data from multi-beam echo-sounders. Because we did not have such measures; we merely employed Yang's equation and performed our tests in a laboratory setting. Additionally, we measured the SSC at each individual section to confirm our estimations of the confluence's suspended load transport rates. In order to quantify daily Qs from Equation (4), it is necessary to calculate annual riverbed height as well as additional daily variables like flow velocity, river width, and cross-sectional area at the three branch channels. The estimations of all these limits were susceptible to potential errors. This is a significant source of uncertainty in the estimations of suspended load in this study. The uncertainty in the average flow rate is governed by errors in the cross-sectional area. The estimation of river width using the earth explorer and arc map tools could lead to inaccuracy in the estimate of cross-sectional area. Additionally, because the stream was assumed to be a rectangle and the cross-sectional areas were calculated as a function of flow depth and channel breadth, the cross-sectional areas at all positions were possibly exaggerated. This study was unable to discover a way to calculate the cross-sectional area such that it perfectly matched the cross-section of the semi-oval riverbed. Although there are certain ambiguities in the study, the estimations of suspended load rates are reasonable.

4. CONCLUSIONS

An instant joining of two channels with separate flow and sediment discharge at a river confluence results in unusual hydro-sediment and morphological conditions. The hydrological conditions of the year and the mixed homogenized area determine the surface water flow and sediment mixing of two distinct upstream channels along the downstream channel. In the current study, two approaches (conventional and empirical) were used to relate sediment concentration and water discharge for better sediment yield estimation. Field surveys were conducted every 2 months intervals through February 2021 and 2022 to investigate the spatiotemporal variations of suspended sediments (suspended sediment transport rate) of a river confluence between the Gumti River and the outflow channel of Pitragang tributary. Bed material and SSC samples were gathered from respective chosen points and analyzed to characterize the samples. A statistical study was applied to assess the accuracy of the approach.

The following highlights could be concluded from this study:

Attempts have been made to investigate the SSL dynamicity of confluence according to field data acquired from the confluence site in order to foresee the impact of a tributary to generate interruption within the longitudinal pattern of suspended load as a function of spatial tributary watershed attribute. The study confirms that the tributary junction reflects locations where the longitudinal gradient of sediment rate changes at specified locations. The tributary has had a significant influence on changing the local sediment discharge of the main channel depending on the size of their catchment corresponding to the main channel. The amount of suspended loads appeared to rise as river discharge and stage increased upstream. At upstream locations, suspended loads appeared to increase with the increasing local suspended particles, river discharge and river stage. The most important issue to control sediment transfer in the CHZ is found to be the sediment output and runoff volume from tributary catchments. The outcome demonstrated that, in many instances

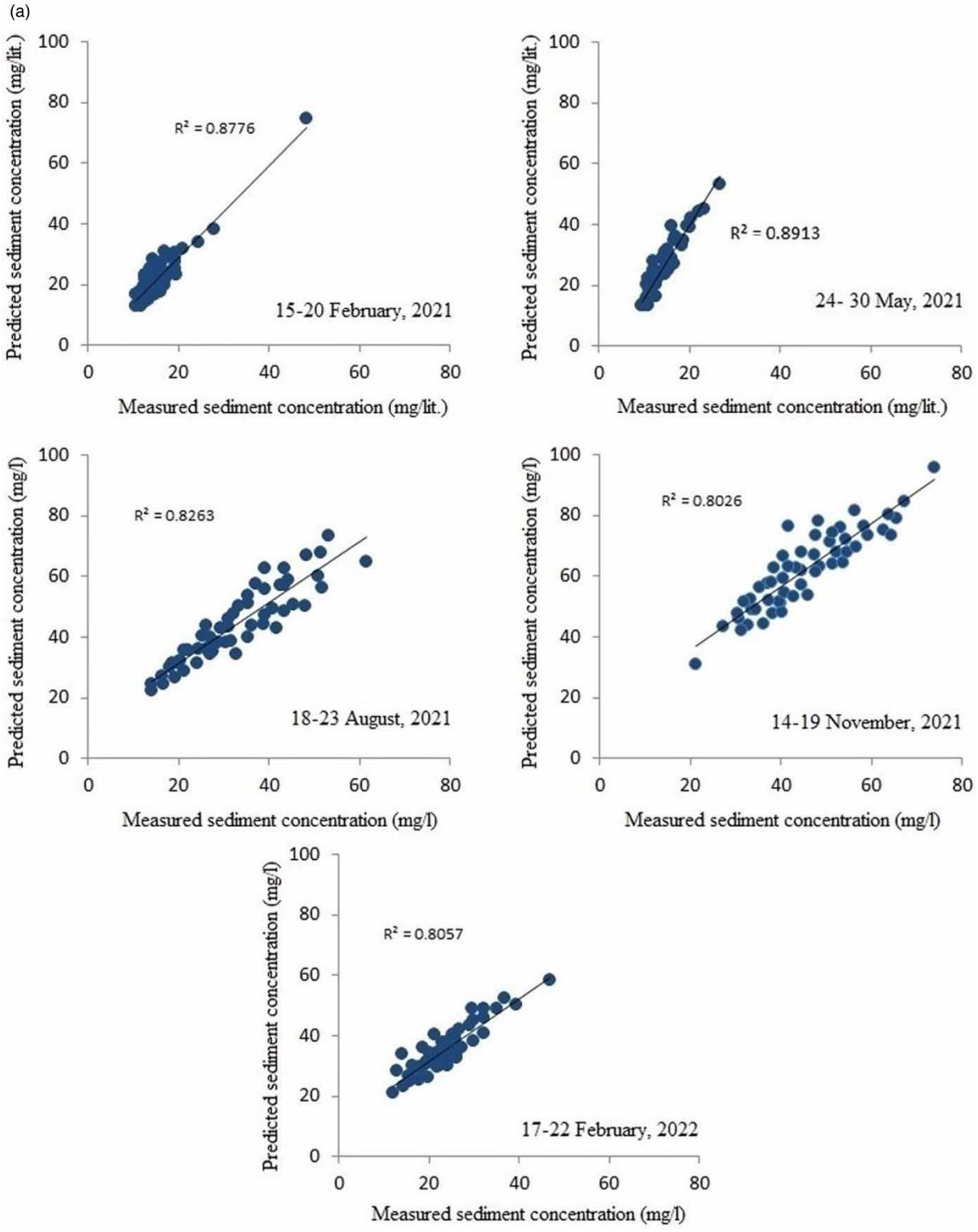

Figure 6 | Display the scatter plot of measured and predicted suspended sediment concentration rate: (a) tributary channel and (b) main channel (d/s). (*continued.*).

correlation coefficient value $R^2 > 0.84$, and the estimated and actual suspended sediment discharge matched well. The measured transport rates of suspended sediment ranged from 642 to 442 g/s, which is in contrast to what Yang's formula computed. This work suggests that a large alluvial river can convey sediment with significant spatiotemporal variability, and that forthcoming sediment management in the stream should discover

(b)

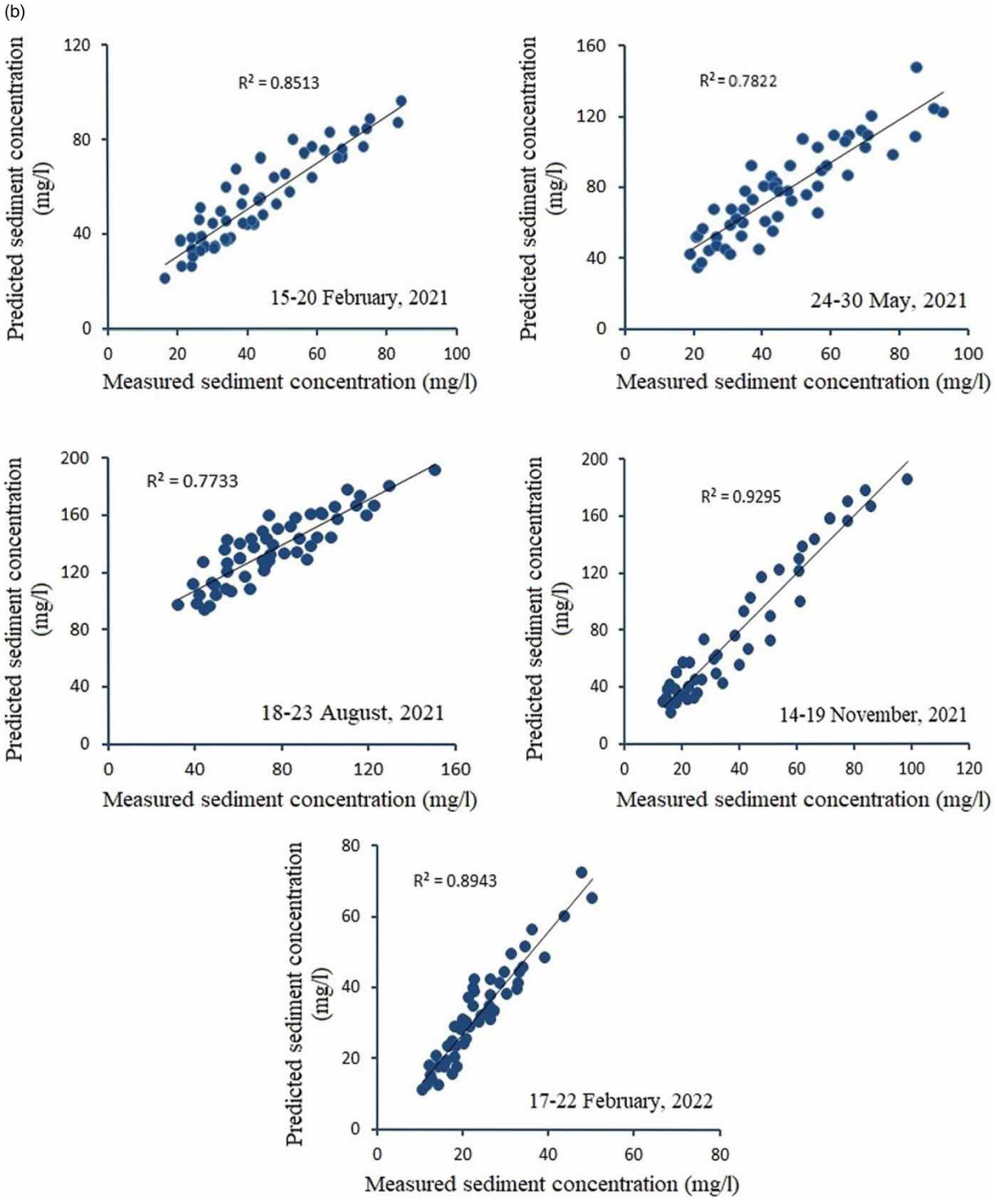

Figure 6 | Continued.

ways to release coarse and fine sediments held in the examined river reach. The results suggest that Yang's formula can be successfully used for the determination of the total sediment concentration in the Gumti River and Pitraganga tributary. Therefore, it is hoped that the work presented here would provide a valuable knowledge basis and inspire creative or innovative ideas for fruitful and cogent future research, particularly in the area of river confluences. From there, future efforts could be focused on managing and restoring the confluences.

ACKNOWLEDGEMENTS

This research was financially supported by the Science and Engineering Research Board (SERB), Ministry of Science and Technology, Government of India (Grant no. EMR/2016/005371).

DATA AVAILABILITY STATEMENT

All relevant data are included in the paper or its Supplementary Information.

CONFLICT OF INTEREST

The authors declare there is no conflict.

REFERENCES

Balouchi, B., Shafai-Bejestan, M., Ruther, N. & Rahmanshahi, M. 2022 Experimental investigation of flow pattern over a fully developed bed at a 60° river confluence in large floods. *Acta Geophysica* **70**(5), 2283–2296.

Baranya, S. N. O. & Jozsa, J. 2013 Flow analysis of a river confluence with field measurements and Rans model with nested grid approach. *River Res. Appl.* **31**, 28–41.

Benda, L., Andras, K., Miller, D. & Bigelow, P. 2004 Confluence effects in rivers: interactions of basin scale, network geometry, and disturbance regimes. *Water Resour. Res.* **40**(5), W05402. https://doi.org/10.1029/2003WR002583.

Biron, P., Lane, S., 2008 Modelling hydraulics and sediment transport at river confluences. In: *River Confluences, Tributaries and the Fluvial Network* (Rice, S. P., Roy, A. G. & Rhoads, B. L. eds.). Wiley & Sons, Ltd, New Jersey, USA, pp. 17–43.

Blettler, M., Amsler, M., Ezcurra de Drago, I., Espinola, L. & Eberle, E. 2014 The impact of significant input of fine sediment on benthic fauna at tributary junctions: A case study of the Bermejo-Paraguay River confluence, Argentina. *Ecohydrology* **8**(2), 340–352.

Cheng, Z. & Constantinescu, G. 2018 Stratification effects on flow hydrodynamics and mixing at a confluence with a highly discordant bed and a relatively low velocity ratio. *Water Resources Research* **54**, 4537–4562. https://doi.org/10.1029/2017WR022292.

Constantinescu, G., Miyawaki, S., Rhoads, B. & Sukhodolov, A. 2012 Numerical analysis of the effect of momentum ratio on the dynamics and sediment entrainment capacity of coherent flow structures at a stream confluence. *Journal of Geophysical Research* **F4**, F04028. https://doi.org/10.1029/2012JF002452.

Constantinescu, G., Miyawaki, S., Rhoads, B. & Sukhodolov, A. 2016 Influence of planform geometry and momentum ratio on thermal mixing at a stream confluence with a concordant bed. *Journal Environmental Fluid Mechanics* **16**(4), 845–873. https://doi.org/10.1007/s10652-016-9457-0.

Duncan, W. W., Poole, G. C. & Meyer, J. L. 2009 Large channel confluences influence geomorphic heterogeneity of a southeastern United States river. *Water Resources Research* **45**(10), W10405. https://doi.org/10.1029/2008WR007454.

Edward, P. & Latrubesse, E. M. 2015 Surface water types and sediment distribution patterns at the confluence of mega rivers: The Solimoes-Amazon and Negro ~ Rivers junction'. *Water Resour. Res.* **51**, 6197–6213. doi:10.1002/2014WR016757.

Escauriaza, C., Gonzalez, C., Guerra, P., Pasten, P. & Pizarro, G. 2012 Formation and fate of contaminant particles controlled by turbulent coherent structures and geochemistry in a reactive river confluence. *Bulletin of the American Physics Society* **57**(17), 7041–7058.

Espinoza, R., Martinez, J. M., Guyot, J. L., Fraizy, P., Armijos, E., Crave, A., Bazán, H., Vauchel, P. & Lavado, W. 2012 The integration of field measurements and satellite observations to determine River solid loads in poorly monitored basins. *J. Hydrol.* **444–445**, 221–228.

Ferguson, R. & Hoey, T. 2008 *Effects of Tributaries on Main-Channel Geomorphology*. John Wiley & Sons, Ltd, Chichester, UK, pp. 183–208.

Gray, J. R. & Simoes, F. J. M., 2008 Estimating sediment discharge, in sedimentation engineering. In: *American Society of Civil Engineering Manuals and Reports on Engineering Practice* (Garcia, M. H. ed.). Reston, VA, ASCE, 54, pp. 1067–1088.

Gray, A. B., Pasternack, G. B., Watson, E. B., Warrick, J. A. & Goni, M. A. 2015 Effects of antecedent hydrologic conditions, time dependence, and climate cycles on the suspended sediment load of the Salinas River, California. *J. Hydrol.* **525**, 632–649.

Gualtieri, C., Filizola, N., de Oliveira, M., Santos, A. M. & Ianniruberto, M. 2018 A field study of the confluence between Negro and Solimoes Rivers. Part 1: Hydrodynamics and sediment transport. *C.R. Geoscience* **350**, 31–42. https://doi.org/10.1016/j.crte.2017.09.015.

Gualtieri, C., Ianniruberto, M. & Filizola, N. 2019 On the mixing of rivers with a difference in density: The case of the Negro/Solimões confluence, Brazil. *Journal of Hydrology* **578**, 124029. https://doi.org/10.1016/j.jhydrol.2019.124029.

Gualtieri, C., Abdi, R., Ianniruberto, M., Filizola, N. & Endreny, T. A. 2020 A 3D analysis of spatial habitat metrics about the confluence of negro and Solimoes rivers, Brazil. *Ecohydrology* **13**(1), 1630. https://doi.org/10.1002/eco.2166.

Guillen Ludena, S., Cheng, Z., Constantinescu, G. & Franca, M. J. 2017 Hydrodynamics of mountain-river confluences and its relationship to sediment transport. *Journal of Geophysical Research: Earth Surface* **122**, 901–924. https://doi.org/10.1002/2016JF004122.

Ianniruberto, M., Trevethan, M., Pinheiro, A., Andrade, J. F., Dantas, E. & Filizola, N. 2018 A field study of the confluence between Negro and Solimoes Rivers. Part 2: Bed morphology and stratigraphy. *Comptes Rendus Geoscience* **350**, 43–54. https://doi.org/10.1016/j.crte.2017.10.005.

Jiang, C., Constantinescu, G., Yuan, S. & Tang, H. 2022 Flow hydrodynamics, density contrast effects and mixing at the confluence between the Yangtze River and the Poyang Lake channel. *Environmental Fluid Mechanics* **00000**, 1–29.

Khanchoul, K., Altschul, R. & Assassi, F. 2009 Estimating suspended sediment yield, sedimentation controls and impacts in the Mellah Catchment of Northern Algeria. *Arab J. Geosci* **2**(3), 257–227.

Khosronejad, A., Le, T., DeWall, P., Bartelt, N., Woldeamlak, S., Yang, X. & Sotiropoulos, F. 2016 High-fidelity numerical modeling of the upper Mississippi river under extreme flood condition. *Advances in Water Resources* **98**, 97–113.

Krause, P., Boyle, D. P. & Base, F. 2005 Comparison of different efficiency criteria for hydrological model assessment. *Adv. Geosci.* **2005**(5), 89–97.

Lane, S. N., Parsons, D. R., Best, J. L., Orfeo, O., Kostachuk, R. & Hardy, R. J. 2008 Causes of rapid mixing at a junction of two large rivers: Rio Paraná and Rio Paraguay, Argentina. *Journal of Geophysical Research* **113**, F02024. https://doi.org/10.1029/2006JF000745.

Leite Ribeiro, M., Blanckaert, K., Roy, A. G. & Schleiss, A. J. 2012 Flow and sediment dynamics in channel confluences. *Journal of Geophysical Research: Earth Surface* **117**(F1). https://doi.org/10.1029/2011JF002171

Lewis, Q., Rhoads, B., Sukhodolov, A. & Constantinescu, G. 2020 Advective lateral transport of streamwise momentum governs mixing at Small River confluences. *Water Resources Research* **56**(9), e2019WR026817.

Lyubimova, T. P., Lepikhin, A. P., Parshakova, Y. N., Kolchanov, V. Y., Gualtieri, C., Roux, B. & Lane, S. N. 2020 A numerical study of the influence of channel-scale secondary circulation on mixing processes downstream of river junctions. *Water* **12**, 2969. https://doi.org/10.3390/w12112969.

Martín-Vide, J. P., Plana-Casado, A., Sambola, A. & Capape, S. 2015 Bed load transport in a river confluence. *Geomorphology* **250**, 15–28. https://doi.org/10.1016/j.geomorph.2015.07.050.

Najafzadeh, M. & Tafarojnoruz, A. 2016 Evaluation of neuro-fuzzy GMDH-based particle swarm optimization to predict longitudinal dispersion coefficient in rivers. *Environ. Earth Sci.* **75**(2), 157. doi:10.1007/s12665-015-4877-6.

Nazari-Giglou, A., Jabbari-Sahebari, A., Shakibaeinia, A. & Borghei, S. M. 2016 An experimental study of sediment transport in channel confluences. *International Journal of Sediment Research* **31**(1), 87–96. https://doi.org/10.1016/j.ijsrc.2014.08.001.

Parsons, D. R., Best, J. L., Lane, S. N., Orfeo, O., Hardy, R. J. & Kostaschuk, R. 2007 Form roughness and the absence of secondary flow in a large confluence-diffluence, Rio Parana, Argentina. *Earth Surf. Processes Landforms* **32**(1), 155–162.

Ragno, N., Redolfi, M. & Tubino, M. 2021 Coupled morphodynamics of river bifurcations and confluences. *Water Resources Research* **57**, e2020WR028515. https://doi.org/10.1029/2020WR028515.

Rhoads, B. L. 2020 *River Dynamics: Geomorphology to Support Management*. Cambridge University Press, Cambridge, UK. https://doi.org/10.1017/9781108164108.

Rhoads, B. L. & Johnson, K. K. 2018 Three-dimensional flow structure, morphodynamics, suspended sediment, and thermal mixing at an asymmetrical river confluence of a straight tributary and curving main channel. *Geomorphology* **323**, 51–69. https://doi.org/10.1016/j.geomorph.2018.09.009.

Rhoads, B. L., Riley, J. D. & Mayer, D. R. 2009 Response of bed morphology and bed material texture to hydrological conditions at an asymmetrical stream confluence. *Geomorphology* **2009**(109), 161–173.

Rice, S. P., Kiffney, P., Greene, C., Pess, G. R., 2008 The ecological importance of tributaries and confluences. In: *River Confluences, Tributaries, and the Fluvial Network* (Rice, S. P., Roy, A. G. & Rhoads, B. L. eds.). John Wiley & Sons Ltd, New Jersey, USA, pp. 209–237.

Riley, J. D., Rhoads, B. L., Parsons, D. R. & Johnson, K. K. 2014 Influence of junction angle on three-dimensional flow structure and bed morphology at confluent meander bends during different hydrological conditions. *Earth Surface Processes and Landforms* **40**, 252–271.

Sukhodolov, A. N. & Sukhodolova, T. A. 2019 Dynamics of flow at concordant gravel bed river confluences: effects of junction angle and momentum flux ratio. *Journal of Geophysical Research: Earth Surface* **124**, 588–615. https://doi.org/10.1029/2018JF004648.

Sukhodolov, A. N., Krick, J., Sukhodolova, T. A., Cheng, Z., Rhoads, B. L. & Constantinescu, G. S. 2017 Turbulent flow structure at a discordant river confluence: Asymmetric jet dynamics with implications for channel morphology. *Journal of Geophysical Research: Earth Surface* **122**(6), 1278–1293. https://doi.org/10.1002/2016JF004126.

Szupiany, R. N., Amsler, M. L., Hernandez, J., Parsons, D. R., Best, J. L., Fornari, E. & Trento, A. 2012 Flow fields, bed shear stresses, and suspended bed sediment dynamics in bifurcations of a large river. *Water Resources Research* **48**(11). doi:10.1029/2011WR011677.

Tachi, S. E., Ouerdachi, L., Remaoun, M., Derdous, O. & Boutaghane, H. 2016 Forecasting suspended sediment load using regularized neural network: Case study of the Isser River (Algeria). *J Water Land Dev* **29**(1), 75–81.

Tang, H., Zhang, H. & Yuan, S. 2018 Hydrodynamics and contaminant transport on a degraded bed at a 90-degree channel confluence. *Environ. Fluid Mech.* **18**, 443–463.

Wang, X., Yan, X., Duan, H., Liu, X. & Huang, E. 2019 Experimental study on the influence of river flow confluences on the open channel stage–discharge relationship. *Hydrological Sci. J.* **64**(16), 2025–2039.

Yang, C. T. 1979 Incipient motion and sediment transport. *J. Hydraul. Div. ASCE* **99**, 1679–1704.

Yu, Q., Yuan, S. & Rennie, C. D. 2020 Experiments on the morphodynamics of open channel confluences: Implications for the accumulation of contaminated sediments. *Journal of Geophysical Research: Earth Surface* **125**, e2019JF005438. https://doi.org/10.1029/2019JF00543.

Yuan, S., Tang, H., Xiao, Y., Qiu, X. & Xia, Y. 2018 Water flow and sediment transport at open-channel confluences: An experimental study. *Journal of Hydraulic Research* **56**, 333–350. https://doi.org/10.1080/00221686.2017.1354932.

Yuan, S., Tang, H., Xiao, Y., Xia, Y., Melching, C. & Li, Z. 2019 Phosphorus contamination of the surface sediment at a river confluence. *Journal of Hydrology* **573**, 568–580. https://doi.org/10.1016/j.jhydrol.2019.02.036.

Yuan, S., Tang, H., Li, K., Xu, L., Xiao, Y., Gualtieri, C., Rennie, C. & Melville, B. 2021 Hydrodynamics, sediment transport and morphological features at the confluence between the Yangtze River and the Poyang Lake. *Water Resources Research* **57**(3), e2020WR028284.

Yuan, S., Xu, L., Tang, H., Xiao, Y. & Gualtieri, C. 2022 The dynamics of river confluences and their effects on the ecology of aquatic environment: A review. *Journal of Hydrodynamics* **34**(1), 1–14.

Zhang, Z. & Lin, Y. 2021 An experimental study on the influence of drastically varying discharge ratios on bed topography and flow structure at urban channel confluences. *Water* **13**(9), Article 9. https://doi.org/10.3390/w13091147.

Zhang, Y., Wang, P., Wu, B. & Hou, S. 2014 An experimental study of fluvial processes at asymmetrical river confluences with hyperconcentrated tributary flows. *Geomorphology* **230**, 26–36.

Zhang, X., Ji, Y., Yang, Z., Wang, Z., Liu, N. & Jia, P. 2015 End member inversion of surface sediment grain size in the South Yellow Sea and its implications for dynamic sedimentary environments. *Sci. China Earth Sci.* **59**, 258–267.

First received 10 November 2023; accepted in revised form 4 February 2024. Available online 28 February 2024